Zitierweise: Angew. Chem. Int. Ed. 2025, 64, e202416700
doi.org/10.1002/anie.202416700

Borazines

Escape from Flatland: Stereoselective Synthesis of Hexa-aryl Borazines and their sp^2-Based 3D Architectures

*Vivek Chandrakant Wakchaure[+], María Mercedes Lorenzo-García[+], Francesco Fasano, Martina Crosta, Nicolas Biot, Nicola Demitri, Pradip Kumar Mondal, Benjamin D. Ward, and Davide Bonifazi**

Abstract: Borazine and its derivatives can be considered critical doping units for engineering hybrid C(sp^2)-based molecules with tailored optoelectronic properties. Herein, we report the first synthesis of hexa-arylborazines that, bearing *ortho*-substituted aryl moieties, extend three-dimensionally. Using a one-pot protocol, we first form an electrophilic chloroborazole and then react it with an aryl lithium (ArLi). By selecting the appropriate *ortho*-substituent, we can guide the ArLi to add to the BN-core in a specific way, ultimately controlling the stereochemical outcome of the three-substitution reaction. Rationalization of the stereochemical model through computational analysis allowed us to show that when aryl lithium nucleophiles bearing rigid long-range *ortho*-substituents are used, i.e., stiff substituents. The *ortho*-substituent shields its side of the electrophilic B_3N_3 core, biasing the incoming ArLi to add *anti* at each addition step, forming the final tri-aryl borazine exclusively as *cc*-isomer. Leveraging this stereoselective approach, prototypical multichromophoric borazine derivatives were prepared, and we showcased how the stereochemical arrangement of these chromophores distinctly influences their redox behavior. This methodology paves the way for previously inaccessible borazines to serve as privileged precursors to transcend the conventional bidimensionality associated with graphenoid systems and pioneer the construction of new forms of three-dimensional C(sp^2)-based architectures.

Introduction

As part of our ongoing project focused on developing synthetic approaches for BN-containing carbon architectures,[1] we have now tackled the synthetic challenges associated with the expansion of the chemical space of the borazine scaffold (Figure 1).[2] Triggered by the vigorous development of the heteroatom-doping approach[3] to tailor the optoelectronic properties of C(sp^2)-based materials, the borazine ring[4] is increasingly attracting the attention of the chemical community[5] to engineer catalysts,[6] polymers,[7] porous materials,[8] and 2D materials.[9] However, the limited comprehension of the reactivity of the B_3N_3 ring and its susceptibility towards hydrolysis have limited the exploitation of borazines as conceptual cores to engineer complex and functional aromatic architectures.[10]

Amongst the different borazines scaffolds, isostructural and isoelectronic congeners of hexaarylbenzenes (HABs),[11] such as propeller-shaped hexaarylborazines (HABNs) (Figure 1), are advantaged chiral molecular modules as they can be easily integrated with HABs to engineer hybrid carbon architectures, including 2D and 3D C(sp^2)-based structures.[12] In particular, HABs and HABNs exposing *ortho*-substituents (*o*Ss) at the radial aryl moieties with restricted rotation (Figure 1) could serve as privileged precursors to transcend the conventional bidimensionality associated with graphenoid systems and pioneer the construction of new forms of three-dimensional[13] C(sp^2)-based architectures. These scaffolds could also serve as platforms for designing functional nanoarchitectures featuring optoelectronic-active groups with different spatial arrangements. For instance, the distinct configurations (e.g., those shown in Figure 1) on the three-dimensional scaffold could offer unprecedented control over chemical reactivity and structural, chiral, and electronic properties. However, to our knowledge, the existing protocols have yet to allow the preparation of either HABs[14] or pyridine-HABs[15] with selected config-

[*] M. M. Lorenzo-García,[+] Dr. F. Fasano, Dr. N. Biot, Dr. B. D. Ward
School of Chemistry, Cardiff University, Main Building, Park Place, Cardiff CF10 3AT, United Kingdom

M. M. Lorenzo-García[+]
Department of Pharmaceutical and Chemical Sciences, University of Trieste, Via Licio Giorgeri 1, Trieste 34127, Italy

Dr. N. Demitri, Dr. P. K. Mondal
Elettra–Sincrotrone, S.S. 14 Km 163.5 in Area Science Park, Basovizza 34149, Trieste, Italy

V. Chandrakant Wakchaure,[+] M. Crosta, Prof. Dr. D. Bonifazi
Institute of Organic Chemistry, Faculty of Chemistry, University of Vienna, Währinger Strasse 38, 1090, Vienna, Austria
E-mail: davide.bonifazi@univie.ac.at

[+] These authors contributed equally to this work.

© 2024 The Author(s). Angewandte Chemie published by Wiley-VCH GmbH. This is an open access article under the terms of the Creative Commons Attribution Non-Commercial License, which permits use, distribution and reproduction in any medium, provided the original work is properly cited and is not used for commercial purposes.

© 2024 The Author(s). Angewandte Chemie published by Wiley-VCH GmbH

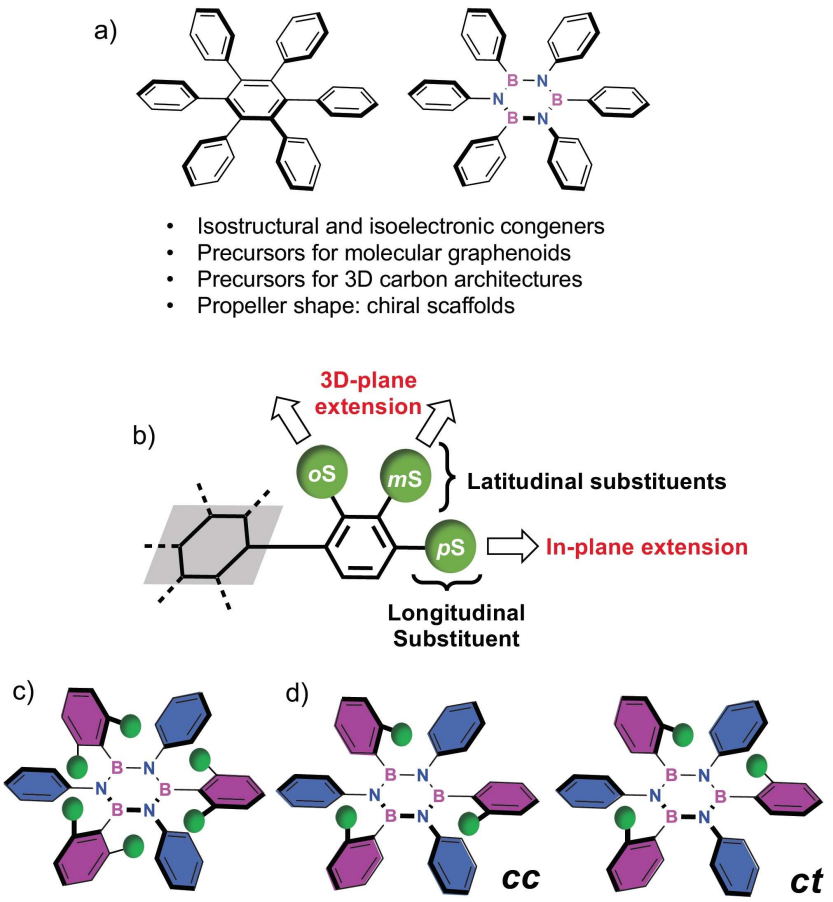

Figure 1. a) Chemical structure of unsubstituted HABs and HABNs. b) Latitudinal (*o*S and *m*S) and longitudinal (*p*S) substituents allowing the 3D and 2D extension. c) Hexa-*o*Ss-aryl borazine. d) Tri-*o*Ss-aryl borazine *cc* and *ct* stereoisomers. *m*S: *meta*-, *p*S: *para*-, and *o*S: *ortho*- substituent; *c*: *cis*, and *t*: *trans*.

urations, and the synthesis efforts thus far have yielded only HABs with enriched isomeric mixtures.

Generally, *N*- and *B*-aryl-substituted borazines[6] are prepared via either dehydrogenation[16] or condensation[17,18,20] reactions from an amine and an electrophilic boron derivative (BX_3, X = H or halogen) that, through the formation of an iminoborane,[18] yield a reactive electrophilic borazine[19] intermediate (Figure 2). Subsequent functionalization at the *B*-atoms can be achieved by successive substitution reactions using organometallic nucleophiles (Figure 2).[18,17] When aniline and BCl_3 are used, the $Cl_3B_3N_3Ph_3$ intermediate is obtained and reacted in situ with ArLi to give the final HABN derivative (Figure 1a).[18b–d] It is conceived that the ArLi attacks the B– Cl groups approaching the B_3N_3 plane to give a sp^3-type boronate intermediate. Final Cl^- elimination gives the BN-substituted aromatic scaffold, with the B_3N_3 ring restoring its planarity. This one-pot protocol can provide access to sterically-congested, hydrolytically-stable borazine architectures (Figure 1b-c)[18b–d,19,20] such as those bearing one or two *ortho*-substituents (*o*Ss) at the radial aryl moieties (Figure 1c and 1d). These molecules are challenging to synthesize when using benzene precursors through metal-catalyzed cross-coupling reactions[21] or following established cycloaddition[22] and cyclotrimerization[23] routes. Considering now HABNs decorated with *B*-aryl moieties bearing only an *o*S with a restricted rotation of the aryl group,[14] these borazines could exist as *cc* (i.e., all *o*Ss are on the same side of the ring) and *ct* (i.e., one *o*S is exposed opposite) stereoisomers (Figure 1c). Building on the stepwise substitution-based mechanism starting from electrophilic $Cl_3B_3N_3Ph_3$ (Figure 2),[18b–d] we inferred that one could control the stereoselectivity of the final product by the appropriate choice of an *o*S on the ArLi. Specifically, if one uses *o*Ss rigid enough to expose a bulky group atop the B_3N_3 core, it should sterically shield one face and bias the stereoselective outcome of each substitution reaction. It is exploiting these principles that in this paper, we describe the stereoselective synthesis of *cc*-HABN derivatives (Figure 2). The *cc*- and *ct*-stereochemical outcome of the reaction is controlled by the structure of the *o*S of the nucleophilic ArLi, with the stiff, shaft-like, long-range moieties such as phenyl, trimethylsilylethynyl, carbazolyl, and fluorenyl groups exclusively affording the *cc*-isomer. Leveraging this stereoselective approach, we prepared prototypical multichromophoric derivatives and show-

© 2024 The Author(s). Angewandte Chemie published by Wiley-VCH GmbH

15213757, 2025, 29, Downloaded from https://onlinelibrary.wiley.com/doi/10.1002/ange.202416700 by Welsh Assembly Government, Wiley Online Library on [21/08/2025]. See the Terms and Conditions (https://onlinelibrary.wiley.com/terms-and-conditions) on Wiley Online Library for rules of use; OA articles are governed by the applicable Creative Commons License

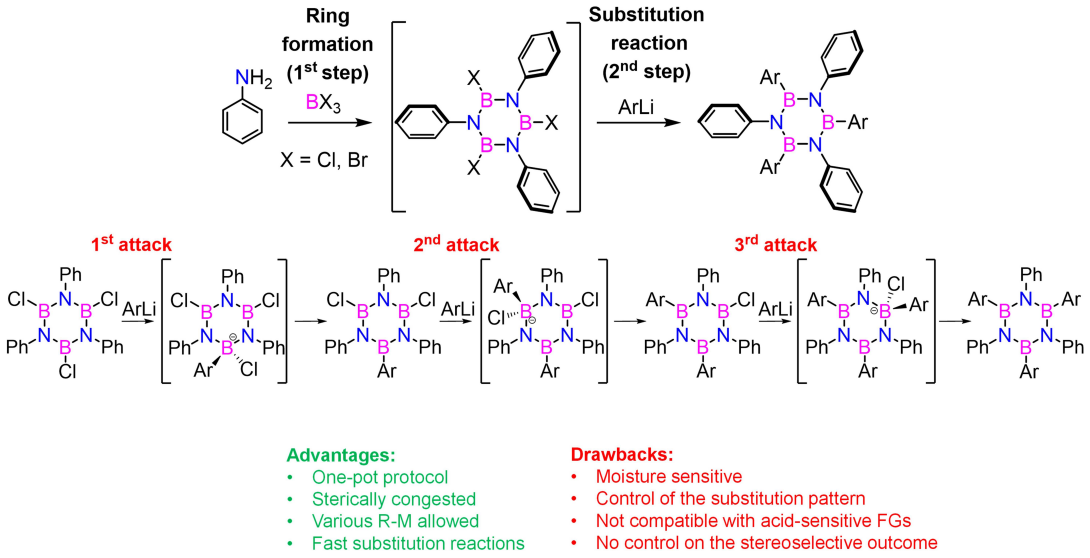

Figure 2. One-pot stepwise synthesis of *N*- and *B*-aryl substituted borazines; step-wise substitutions on a $Cl_3B_3N_3Ph_3$ involving borate intermediates.

cased how the stereochemical arrangement of these chromophores distinctly influences their redox behavior.

Results and Discussion: Synthesis and Structural Analysis

All borazines were prepared following the one-pot BCl_3/$PhNH_2$/ArLi protocol.[18b–d,20] Building on the hypotheses mentioned above, we envisioned using ArLi bearing three types of *o*Ss (Table 1): short-range (SR*o*Ss), π-extended (π-E*o*S), and long-range (LR*o*Ss). The former bears the hindering moiety close to the C(sp^2)– Li bond. In LR*o*Ss, the substituent is constituted by a shaft-like moiety that rigidly points inwards onto the borazine face (i.e., phenyl, ethynyl, and ethenyl spacers). In contrast, the π-E*o*Ss bear benzene moieties linearly fused in an acene-type fashion and extend perpendicularly to the borazine plane. When using ArLi bearing either an OMe or a Me *o*Ss (entries 1–2), borazines **1** and **2** were obtained, each in a *cc*:*ct* 1:≤4 ratio. Similar results were observed with either 4-*tert*-butyl- or 4-chloro-anilines (Table S3.1). When raising the steric hindrance of the SR*o*S to NMe_2 and *i*Pr, a noticeable lowering of the *cc*:*ct* ratio to 12:88 and 10:90 was observed for products **3** and **4**, respectively (entries 3–4). Notably, when using ArLi bearing a *t*Bu, we could not isolate the corresponding borazine **5**, due to the presence of higher steric hindrance of *ortho*-substituents. When using 1-naphthyl and 2-anthracenyl lithium, three-substituted borazines **6** and **7** were obtained (entries 6 and 7) in a statistical *cc*:*ct* 1:3 isomeric mixture.

Next, we turned our attention to ArLi bearing LR*o*Ss. Organolithium derivatives bearing an *ortho*-phenyl moiety (entry 8) exclusively yielded borazine ***cc*-8a** in 63 %, as ultimately confirmed by X-ray diffraction analysis (Figure 3a). Reference reactions performed with ArLi bearing an *ortho*-4-toluoyl also gave the *cc*-isomer (***cc*-8b**) (SI). The addition of ArLi nucleophile-bearing *ortho*-trimethylsilyl ethynyl (TMSE), *ortho*-phenyl ethynyl (PhE), and *ortho*-triisopropylsilylethynyl (TIPSE) LR*o*Ss were also studied. These ArLi derivatives gave borazines ***cc*-9** (63 %), ***cc*-10** (62 %), and ***ct*-11** (40 %) as unique stereoisomers (entries 9–11). While characterizing the products, it was noticed that, upon heating, isomers ***cc*-9** and ***cc*-10** irreversibly converted into ***ct*-9** and ***ct*-10**, respectively (see also the discussion below, Figure 4).

The structural identities of ***cc*-9** (Figure 4a), ***ct*-9** (Figure 4b), ***ct*-10** (Figure 3b), and ***ct*-11** (Figure 3c) were finally confirmed by X-ray diffraction analysis.[24] While ***cc*-9** features all *o*Ss on the same side of the B_3N_3 core, in ***ct*-9**, ***ct*-10**, and ***ct*-11**, one *o*S stands on the opposite side. At the solid state, the structure of ***ct*-10** displays the phenyl moiety in *trans*, perfectly centered atop the B_3N_3 ring in an edge-to-face conformation. In contrast, the two *cis* phenyl moieties engage in intramolecularly π-π stacking (Figure 3b). Consistently, ArLi bearing *E*-vinyl phenyl (P_EV) and triazene substituents (entries 12–13) gave borazines ***cc*-12** and ***cc*-13**. Again, the *cc* configuration was confirmed by X-ray analysis (Figure 3d-e),[24] which depicted the *cis* arrangement for the three substituents. Notably, in both crystals of ***cc*-12** and ***cc*-13**, one of the three vinyl and triazene linkers adopts an *in*-type conformation. While in ***cc*-11**, the conformation is driven by a C-H···π interaction, in ***cc*-13**, it is a short N···B contact (2.690 Å) that turns one triazene moiety in the *in*-type conformation. Obviously, in all *cc*-isomers, both *M* and *P* helicities were found in the solid state (see also Figure S6.1-S6.4). Finally, ArLi bearing a *Z*-vinylphenyl (P_ZV) substituent (entry 14) gave corresponding borazine **14** as a mixture of *cc*- and *ct*-isomers.

© 2024 The Author(s). Angewandte Chemie published by Wiley-VCH GmbH

15213757, 2025, 29, Downloaded from https://onlinelibrary.wiley.com/doi/10.1002/ange.202416700 by Welsh Assembly Government, Wiley Online Library on [21/08/2025]. See the Terms and Conditions (https://onlinelibrary.wiley.com/terms-and-conditions) on Wiley Online Library for rules of use; OA articles are governed by the applicable Creative Commons License

Table 1: Study of the substituent-dependent reaction stereoselectivity. The yields for all molecules referred to the isolated product, whereas the isomer ratio is calculated from the ^{1}H-NMR spectra (see Table S3.2). 4-^{t}Bu-aniline was used for entry **13**. [a]Irreversible.

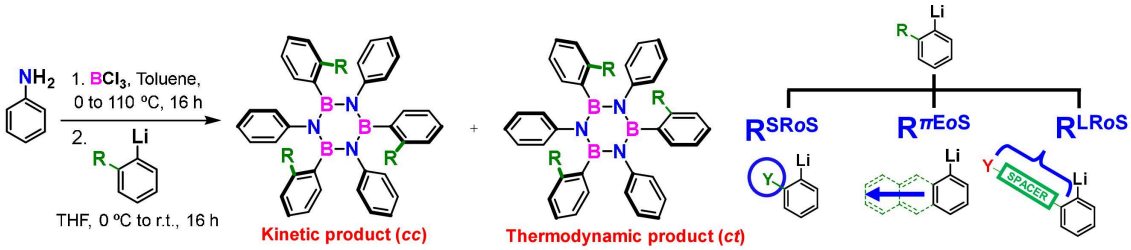

Entry	Type	ArLi	Product (Yield)	*cc:ct*	Entry	Type	ArLi	Product (Yield)	*cc:ct*
1	SRoS		**1** (69%)	18:82	8	LRoS	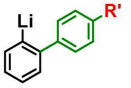	**8a** R' = H; (63%) **8b** R' = Me; (70%)	100:00
2			**2** (69%)	22:78	9		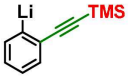	**9** (63%)	100:0 → 0:100[a]
3		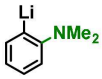	**3** (47%)	12:88	10		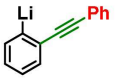	**10** (62%)	100:0 → 0:100[a]
4			**4** (60%)	10:90	11		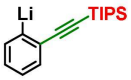	**11** (40%)	0:100
5			**5** (0%)	-	12		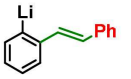	**12** (63%)	100:0
6	πEoS		**6** (53%)	25:75	13		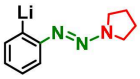	**13** (55%)	100:0
7		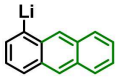	**7** (32%)	25:75	14		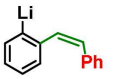	**14** (52%)	mixture

Configurational stability

We performed variable temperature (VT) ^{1}H NMR measurements to investigate the different stereoisomers' stability. While no changes of the stereoisomeric ratio were observed experimentally for molecules **1–8** and **11–14** upon heating (see Figure S3.4-S3.6), only borazines **9** and **10** displayed a complete *cc*→*ct* conversion. For instance, when a solution of ***cc*-9** was heated to 50 °C, a progressive decrease of the intensity of the TMS-proton singlet resonance at 0.44 ppm was observed (Figure 5a) together with a rise of another TMS-centered 1:2 two-singlet pattern typical of the *ct* isomer (at 0.49 and 0.53 ppm, *cc*:*ct* ratio of 9:91 after 155 min). Reverse cooling to rt did not affect the stereoisomeric composition, suggesting that the reaction is irreversible and ***ct*-9** is the thermodynamic product. The isomerization reaction's free-energy activation ($\Delta G^{\neq}$) was experimentally estimated to be ca. 24 kcal mol^{-1} ($k = 2{\cdot}10^{-4}$ s^{-1}) at 323 K. Single-point calculations of the optimized configurational structures of **9** in the gas phase (Figure 5b) further confirmed that isomer ***ct*-9** is more stable than ***cc*-9** ($\Delta\Delta G^0 = -4.9$ kcal mol^{-1}), suggesting that the rotation of the substituent around the aryl C(sp^2)–B bond release the high-energy steric congestion between the TMS groups in ***cc*-9** giving the thermodynamic product. Excluding a B_3N_3-opening/B_3N_3-closing mechanism (Figure S3.3), the *cc*→*ct* isomerization mechanism was probed using DFT calculations. A relaxed potential energy surface (PES) scan of one N–B–C^1–C^2 dihedral angle for the *ct*→*cc* transformations in both the *ortho*-tolyl (**2**) and *ortho*-alkynyl (**9**) derivatives allowed us to estimate the extent of the borazine ring deformation and the barrier to interconversion. The relative electronic energies are shown in Figure 5c and indicate a high barrier to rotation (ca. 23 kcal mol^{-1} and 30 kcal mol^{-1} at r.t. for **2** and **9**, respectively). As expected, rotating the aryl substituent into the borazine ring's plane gives a maximum energy profile corresponding to a puckering of the borazine ring. This can be quantified by considering the RMS deviation of the boron atoms from a plane defined by the three N atoms. Borazine **2** gives RMSD = 0.175 Å at the energy maximum, comparable to that seen in congener **9** (0.178 Å). For molecule **2**, the energy maximum lies with the rotating ring approximately coplanar to the borazine, i.e., a 0° N–B–C_{ipso}–C dihedral angle. However, the toluoyl ring was found to be somewhat

© 2024 The Author(s). Angewandte Chemie published by Wiley-VCH GmbH

15213757, 2025, 29, Downloaded from https://onlinelibrary.wiley.com/doi/10.1002/ange.202416700 by Welsh Assembly Government, Wiley Online Library on [21/08/2025]. See the Terms and Conditions (https://onlinelibrary.wiley.com/terms-and-conditions) on Wiley Online Library for rules of use; OA articles are governed by the applicable Creative Commons License

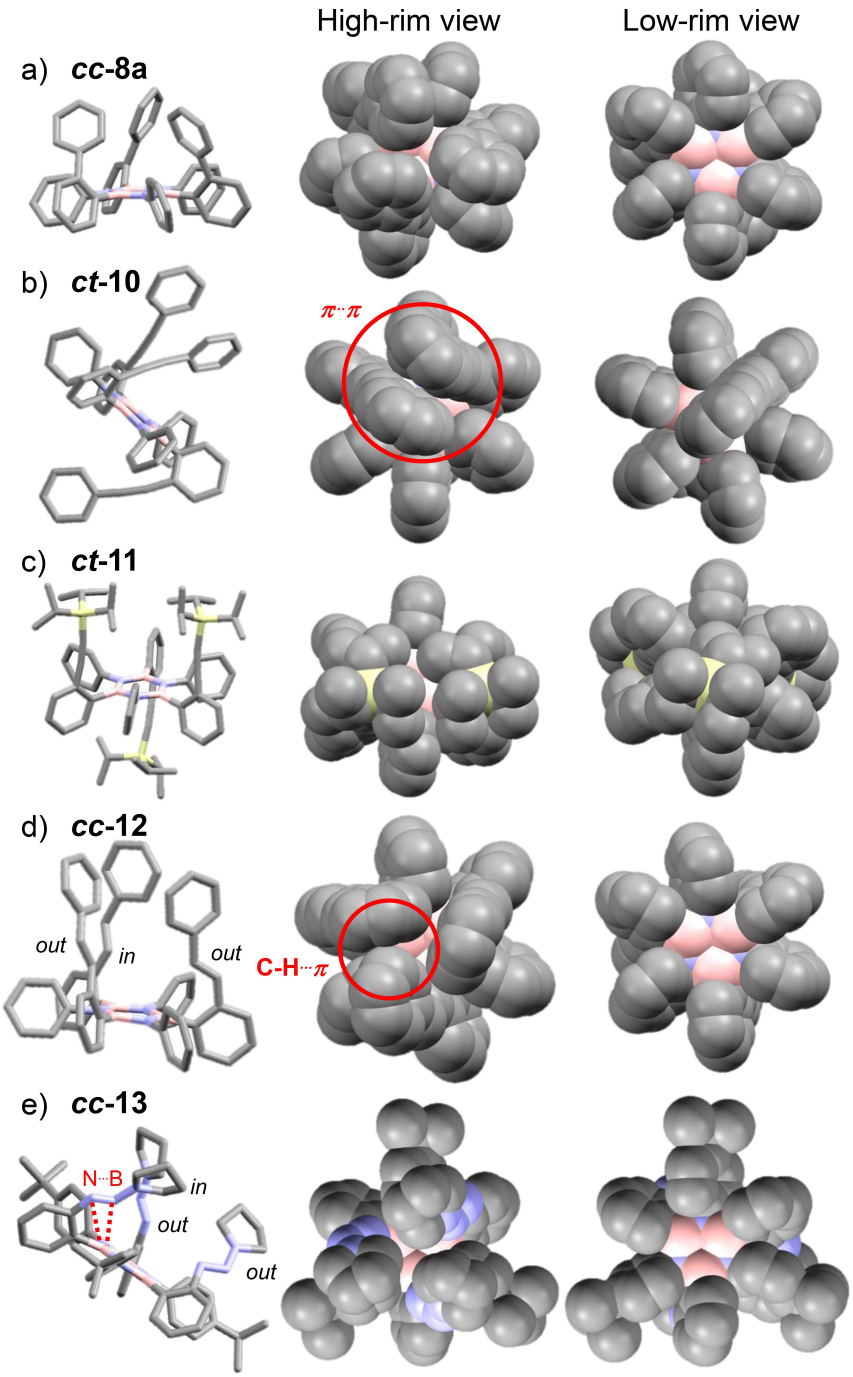

Figure 3. Single-crystal X-ray structure of borazines: a) ***cc*-8a** (*P*-1), b) ***ct*-10** ($P2_1/n$), c) ***ct*-11** ($P2_1/n$), d) ***cc*-12** (*P*-1) and e) ***cc*-13** (*P*-1). Crystals were grown by slow diffusion of MeOH or *i*PrOH in $CHCl_3$ or CH_2Cl_2. In ***cc*-13**, two phenyl moieties engage in a C-H···π interaction (3.369 Å). Grey: C, pink: B, blue: N and yellow: Si.

distorted via a bend in the *ortho*-methyl substituent; the C^5– C^2– Me angle was measured as 165.4°, substantially deviating from the expected 180°. For molecule **9**, the PES energy profile is less symmetrical (Figure 5c) than that observed with the tolyl substituents; the energy profile gradually increases, reaching a maximum with the N– B– C^1– C^2 dihedral angle at approximately +10° (i.e. with the aryl group rotated beyond the expected coplanar arrangement) before rapidly decreasing. Compared to the tolyl substituent, the aryl ring distortion at the energy maximum is increased, with a C^5–C^2–C^{alkyne} angle of 159.9°. Natural bonding orbital (NBO) analysis of the structure corresponding to the energy maximum revealed a substantial reduction of the delocalization of the alkynyl spacer. Each of the "perpendicular" alkyne groups (i.e., those not involved in the PES) shows a significant donor-acceptor interaction between a C^2-based lone pair and an alkyne-based π* (Figure 5c-left). This interaction is absent

© 2024 The Author(s). Angewandte Chemie published by Wiley-VCH GmbH

15213757, 2025, 29, Downloaded from https://onlinelibrary.wiley.com/doi/10.1002/ange.202416700 by Welsh Assembly Government, Wiley Online Library on [21/08/2025]. See the Terms and Conditions (https://onlinelibrary.wiley.com/terms-and-conditions) on Wiley Online Library for rules of use; OA articles are governed by the applicable Creative Commons License

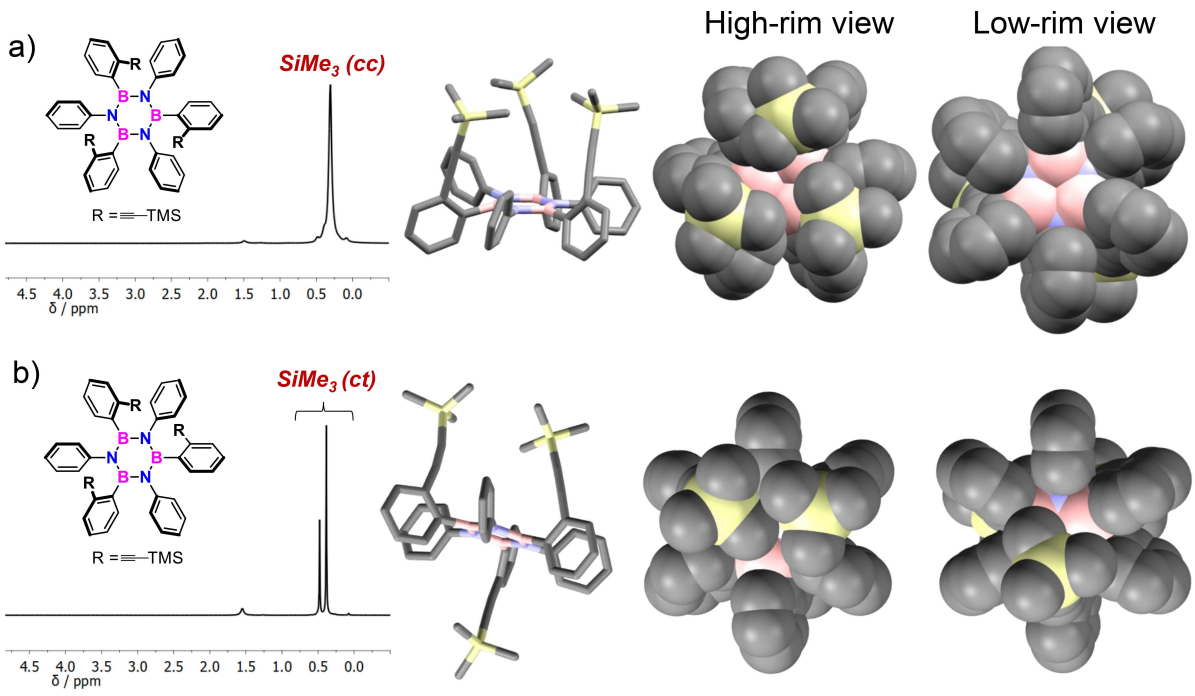

Figure 4. 400-MHz ^{1}H-NMR in $CDCl_3$ and single-crystal X-ray structures of a) ***cc*-9** ($P2_1$), b) ***ct*-9** ($Pna2_1$), with ***ct*-9** obtained by heating a solution of ***cc*-9**. Crystals were grown by slow diffusion of *i*PrOH in either $CHCl_3$ or CH_2Cl_2, with those of ***cc*-9** obtained at 4-11°C to avoid isomerization. Grey: C, pink: B, blue: N and yellow: Si.

from the alkyne substituent of the "coplanar" aryl group, with only weak $\sigma\rightarrow\sigma^*$ and $\sigma\rightarrow\pi^*$ interactions found (Figure 5c-right, see ESI Figure S4.1-S4.4, Table S4.1-S4.5 for full details). This loss of delocalization via distortion of the alkynyl group is presumably the major contributor to the higher activation barrier for the alkynyl vs. tolyl derivative since the borazine ring distortion is comparable regardless of the identity of the *ortho*-substituent.

In the case of **11**, the solely isolated *ct* derivative is − 8.9 kcal mol^{-1} more stable than its hypothetical *cc* isomer. Therefore, it is suggested that, in this case, the reaction is under complete thermodynamic control, with the *cc*-isomer likely undergoing instantaneous isomerization into the *ct* derivative. At last, minimal differences in the $\Delta\Delta G^0$ between the *cc* and *ct* isomers for borazines **1–4** and **8** were theoretically estimated, with 1.7, 1.1, − 0.6, − 2.3, − 0.8 kcal mol^{-1} in difference (see Table S4.1). These studies suggested that the borazine derivatives can undergo isomerization reactions through a rotation around the C(sp^2)– B, the energy barrier of which depends on the *oS*. All *oS*s, but that bearing a phenyl spacer, feature a sufficiently low energy barrier to induce the rotation about the C(sp^2)– B bond by heating. A change of effective isomerization is substantially observed only for those systems in which the *cc* and *ct* isomers have different thermodynamical stability. This suggests that, although for molecule **6**, the rotation of the B-Aryl moieties occurs upon heating, the *cc*:*ct* ratio does not change for statistical reasons (Figure S3.6). On the other hand, for molecule **11**, the significant thermodynamic difference between the *cc*- and *ct*-isomers did not allow the isolation of the least stable *cc*-isomer.

Mechanistic rationale for the cc-stereoselectivity

To shed further light on the stereoselective nature of the substitution and elimination reactions, we used DFT calculations to simulate the rotation of the aryl groups and the nature and energies of the transition states and intermediates arising from the nucleophilic substitution steps (the Gibbs free energies of the transition states, relative to the preceding borazine, i.e., $B_3N_3Cl_3$ for **TS1**, $B_3N_3Cl_2Ar$ for **TS2**, and $B_3N_3ClAr_2$ for **TS3** are in Table 2, see also the Supporting Information section 4 for additional details). For clarity and brevity, only the computed Gibbs free energy profiles for the stereoselective formation of ***cc*-8a** and ***ct*-8a** are shown in Figures 6a and S4.5, respectively.

Specifically, after the first substitution reaction (TS1), in TS2, there is a clear favoring of the *anti-out* approach for the ArLi bearing the phenyl substituent, whereas similar activations energies were computed with the tolyl moieties; this is expected to afford the *cis* isomer as the predominant intermediate under kinetic control for the phenyl substituent in contrast to the tolyl that should give a mixture of isomers. In TS3, *anti*-addition is favored, which is expected by simple steric arguments. The dominance of the *cis* isomer from the second addition for the phenyl-bearing intermediate would reduce the number of viable trajectories in the third addition to mainly *syn*-

© 2024 The Author(s). Angewandte Chemie published by Wiley-VCH GmbH

15213757, 2025, 29, Downloaded from https://onlinelibrary.wiley.com/doi/10.1002/ange.202416700 by Welsh Assembly Government, Wiley Online Library on [21/08/2025]. See the Terms and Conditions (https://onlinelibrary.wiley.com/terms-and-conditions) on Wiley Online Library for rules of use; OA articles are governed by the applicable Creative Commons License

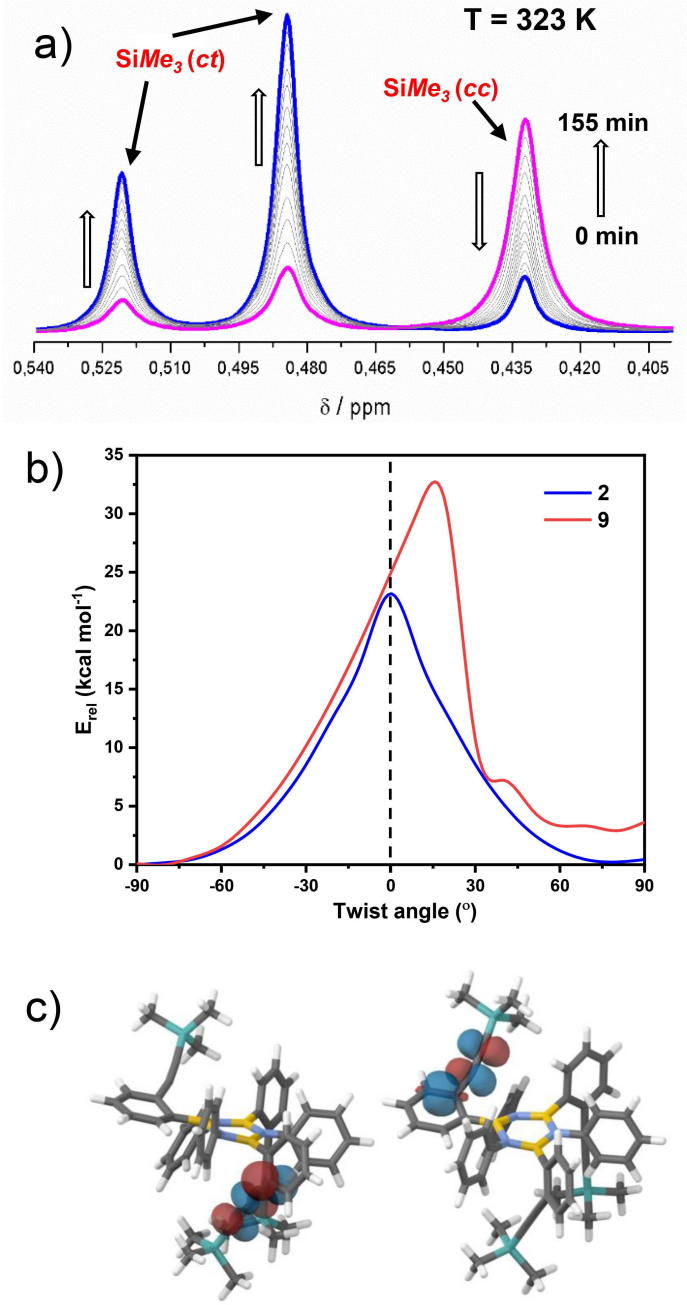

Figure 5. a) Time-dependent ^{1}H NMR investigations of the ***cc*-9→*ct*-9** isomerization at 50 °C. b) Isomerization energy diagram for the *cc*→*ct* transformations for molecules **2** and **9** as a function of the N–B–C–C dihedral angle (structures optimized with a fixed N–B–C^{1}–C^{2} angle in steps of 10° starting from –90°). c) Borazine **9** corresponding to the energy maximum upon twisting one alkynylphenyl ring, showing the donor-acceptor interactions associated with delocalization about the alkyne (left) perpendicular and (right) parallel to the borazine core obtained at the [B3LYP | 6–31 + G(d,p)] level of theory.

syn and *anti-anti*. Of the two trajectories, the *anti-anti* approach is favored ($\Delta G^{\ddagger} = 16.6$ kcal mol^{-1} vs. 20.9 kcal mol^{-1} and 19.4 kcal mol^{-1} for the *syn-syn* and *syn-anti* approaches, respectively), and the *out* conformation is the only viable transition state. It is expected to lead to the exclusive formation of the *cc*-isomer (Figure 6a) as observed experimentally (Table 1, entry 8).

As far as the tolyl case is concerned, the narrower differences in energy between the transition states ($\Delta\Delta G^{\ddagger}$ < 1.5 kcal mol^{-1}) suggest that *ct*:*cc* mixtures are likely to be obtained, in agreement with the observed reaction outcome (Table 1, entry 2). Thus, the overall picture generated from the computational analysis is that when ArLi-bearing LR*o*Ss are used, the substituents shield their side of the electrophilic B_3N_3 core, biasing the incoming ArLi to exclusively add in *out-anti* at the 2nd attack, directing the LR*o*S to a *cis*-relationship in the bis-aryl intermediate. At the 3rd attack, the ArLi also adds *out-anti-anti*, forming

© 2024 The Author(s). Angewandte Chemie published by Wiley-VCH GmbH

15213757, 2025, 29, Downloaded from https://onlinelibrary.wiley.com/doi/10.1002/ange.202416700 by Welsh Assembly Government, Wiley Online Library on [21/08/2025]. See the Terms and Conditions (https://onlinelibrary.wiley.com/terms-and-conditions) on Wiley Online Library for rules of use; OA articles are governed by the applicable Creative Commons License

Table 2: Relative $\Delta G^{\ddagger}$ [$\Delta G^{\ominus}$] energies (kcal mol^{-1}) calculated at the B3LYP | 6–31 + G(d,p) level of theory between the given transition state and the preceding reactive intermediate (i.e., $\Delta G(TS1)^{\ddagger} = \Delta G(TS1) - \Delta G(SM)$, $\Delta\Delta G^{\ominus}$ of the anionic boronate intermediate).

	Approaching side	*in/out*	R = Me	R = Ph	Isomerism
TS1	–	*in*	14.3 (–23.8)	–	–
	–	*out*	14.7 (–23.8)	12.7 (–20.7)	–
TS2	*syn*	*in*	16.2 (nd)[a]	–	*c*
	syn	*out*	15.9 (nd)[a]	16.7 (–14.6)	*t*
	anti	*in*	16.3 (–21.4)	–	*t*
	anti	*out*	15.0 (–21.4)	13.4 (–15.5)	*c*
TS3	*syn-syn*	*in*	19.8 (–14.5)	–	*cc*
	syn-syn	*out*	19.0 (–14.5)	20.9 (–8.1)	*ct*
	syn-anti	*in*	18.1 (–15.8)	–	*ct*
	syn-anti	*out*	17.1 (–15.8)	19.4 (nd)[a]	*ct*
	anti-anti	*in*	18.1 (–15.9)	–	*ct*
	anti-anti	*out*	16.6 (–15.9)	16.6 (–12.2)	*cc*

[a] $\Delta G^{\ominus}$ Value not determined since geometry optimization of the anionic product spontaneously eliminated chloride.

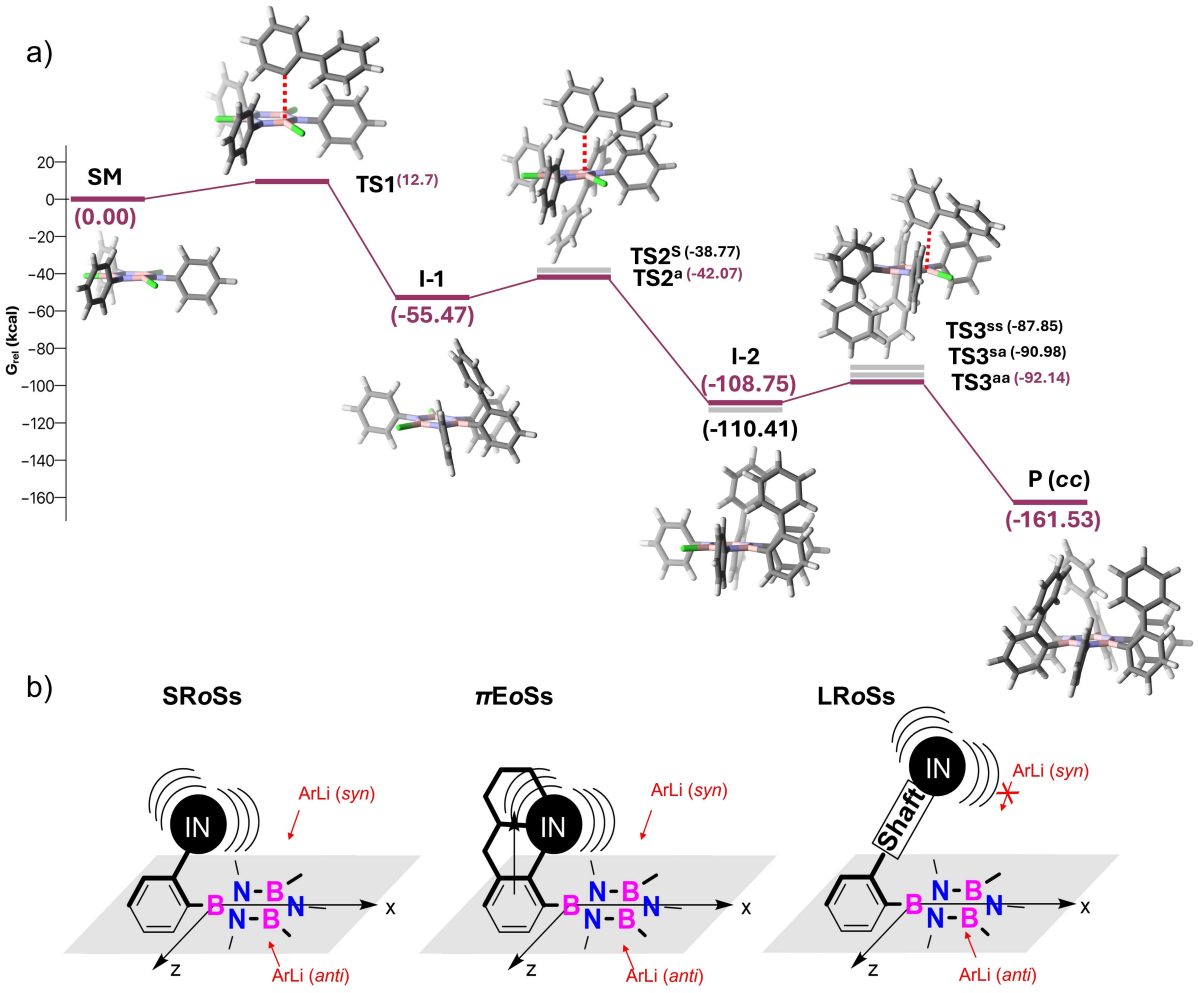

Figure 6. a) Gibbs free energy profiles (kcal mol^{-1}) for the formation of ***cc*-8a** in THF as calculated at the B3LYP | 6–31 + G(d,p) level of theory. b) Conceptualization of the stiff-substituent shielding effect with LRoSs, constituted by a shaft-like moiety that rigidly points a substituent inwards onto the borazine (name inspired by tactic in American football and Rugby called "stiff-arm fend," employed by the ball carrier in many contact forms).

the final tri-aryl borazine exclusively as *cc*-isomer. As expected, the stiff-arm shielding effect is lost when LR*o*Ss are built with a *z*-vinyl shaft. This moiety slips outward the borazine ring, suppressing the facial selectivity for the ArLi to add *anti*. Similarly, complete control of stereoselectivity is lost when π*E*oS and SR*o*S are used, as those

© 2024 The Author(s). Angewandte Chemie published by Wiley-VCH GmbH

15213757, 2025, 29, Downloaded from https://onlinelibrary.wiley.com/doi/10.1002/ange.202416700 by Welsh Assembly Government, Wiley Online Library on [21/08/2025]. See the Terms and Conditions (https://onlinelibrary.wiley.com/terms-and-conditions) on Wiley Online Library for rules of use; OA articles are governed by the applicable Creative Commons License

do not fully shield the electrophilic B_3N_3 ring. While the πE*o*S gave statistical mixtures (*cc*:*ct* of 1:3), different mixtures of *cc* and *ct* are obtained with SR*o*S depending on the *ortho*-substituents.

cc-Stereoselectivity: Substrate scope

As ArLi derivatives bearing an *ortho*-Ph moiety (Table 1, entry 8) exclusively yielded HABNs with *cis*-stereoselectivity, we decided to capitalize on such a *cis*-directing effect to expand the substrate scope of these *cc*-HABNs. Thus, we first exploited the *ortho*-phenyl moiety to spatially direct *m*Ss (entries 1–3, Table 3).

When equipping the *ortho*-substituted ArLi derivatives with -N(Me)$_2$ (entry 1), -TMSE (entry 2) and N,N-dimethylaniline-ethynyl (DMAE) moieties (entry 3) at the *meta*-position, *cc*-isomers exposing the *ortho*-phenyl rings and the *meta*-substituents on higher and lower rims, respectively, were uniquely obtained in high yields (54 % and 49 % yield for ***cc*-8c** and ***cc*-8d**, respectively).

Interestingly, deprotection of the TMS group in ***cc*-8d** with K_2CO_3 in MeOH gave terminal acetylene ***cc*-8f** in 93 % yield, in which the *cc* stereochemistry is maintained. X-ray analysis of single crystals of ***cc*-8c**, ***cc*-8d**, and ***cc*-8f** further confirmed their *cc*-isomerism (Figure 7),[24] with the *ortho*-phenyl and *meta*-substituents groups positioned on the same and opposite sides of the B_3N_3 core, respectively. Considering the high *cc*-stereoselectivity of the biaryl organolithium derivatives, we hypothesized that organolithiums bearing fused aryl rings (FANs), such as carbazole (entry 4), fluorene (entry 5) and spirobi-(fluorene) (entry 6), could also exclusively lead to the formation of *cc*-borazines. Interestingly, the carbazole moiety gave the *cc*-isomer in good yields independently on the substituent (between 46 and 62 %), whereas fluorene provided configurationally stable borazine derivatives (**19**) only with the spirobi(fluorene) moieties. All borazines are configurationally stable at rt, except for borazine **18** (bearing fluorenyl moieties), which undergoes *cc*→*ct* isomerization during the purification (see S5.35). Single crystals suitable for X-ray analysis were grown for ***cc*-17b** (Figure 7d) and ***cc*-19** (Figure 7e), and their *cc*-configuration was confirmed.[24]

Towards functional architectures: Multichromophoric molecular electron storages

Capitalizing on the possibility of installing substituents in the higher or lower rim, we conjectured that such *cc*-borazines could serve as suitable scaffolds to position electroactive moieties in proximity or far and create a

Table 3: Synthesis of *cc*-borazine derivatives exploiting a Ph and fused aryl rings directing group. The yields for all molecules are referred to as the isolated product; SANs: *m*-substituted aryl rings; FANs: fused aryl rings.

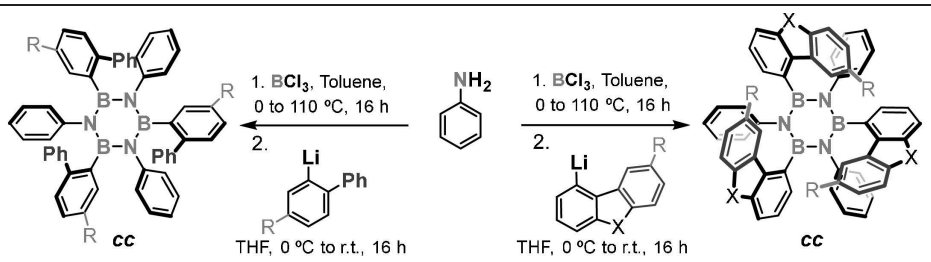

Entry	Type	ArLi	Product (Yield)	Entry	Type	ArLi	Product (Yield)
1	SANs	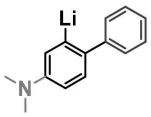	**8c** (54%)	4	FANs	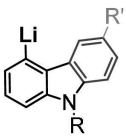	**17a**, R= Me, R'= H; (54%) **17b**, R= -nC_6H_{13}, R'= H; (46%) **17c**, R= -nC_6H_{13}, R'= ≡—TMS; (62 %)
2	SANs	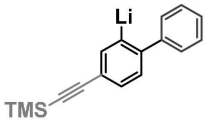	**8d** (49%)	5	FANs	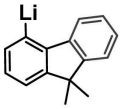	**18** (36%)
3	SANs	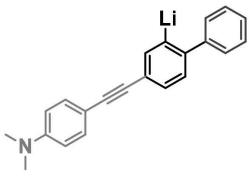	**8e**[a]	6	FANs	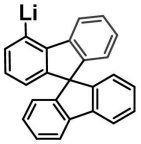	**19** (57%)

[a] Perform next step without isolation

© 2024 The Author(s). Angewandte Chemie published by Wiley-VCH GmbH

15213757, 2025, 29, Downloaded from https://onlinelibrary.wiley.com/doi/10.1002/ange.202416700 by Welsh Assembly Government, Wiley Online Library on [21/08/2025]. See the Terms and Conditions (https://onlinelibrary.wiley.com/terms-and-conditions) on Wiley Online Library for rules of use; OA articles are governed by the applicable Creative Commons License

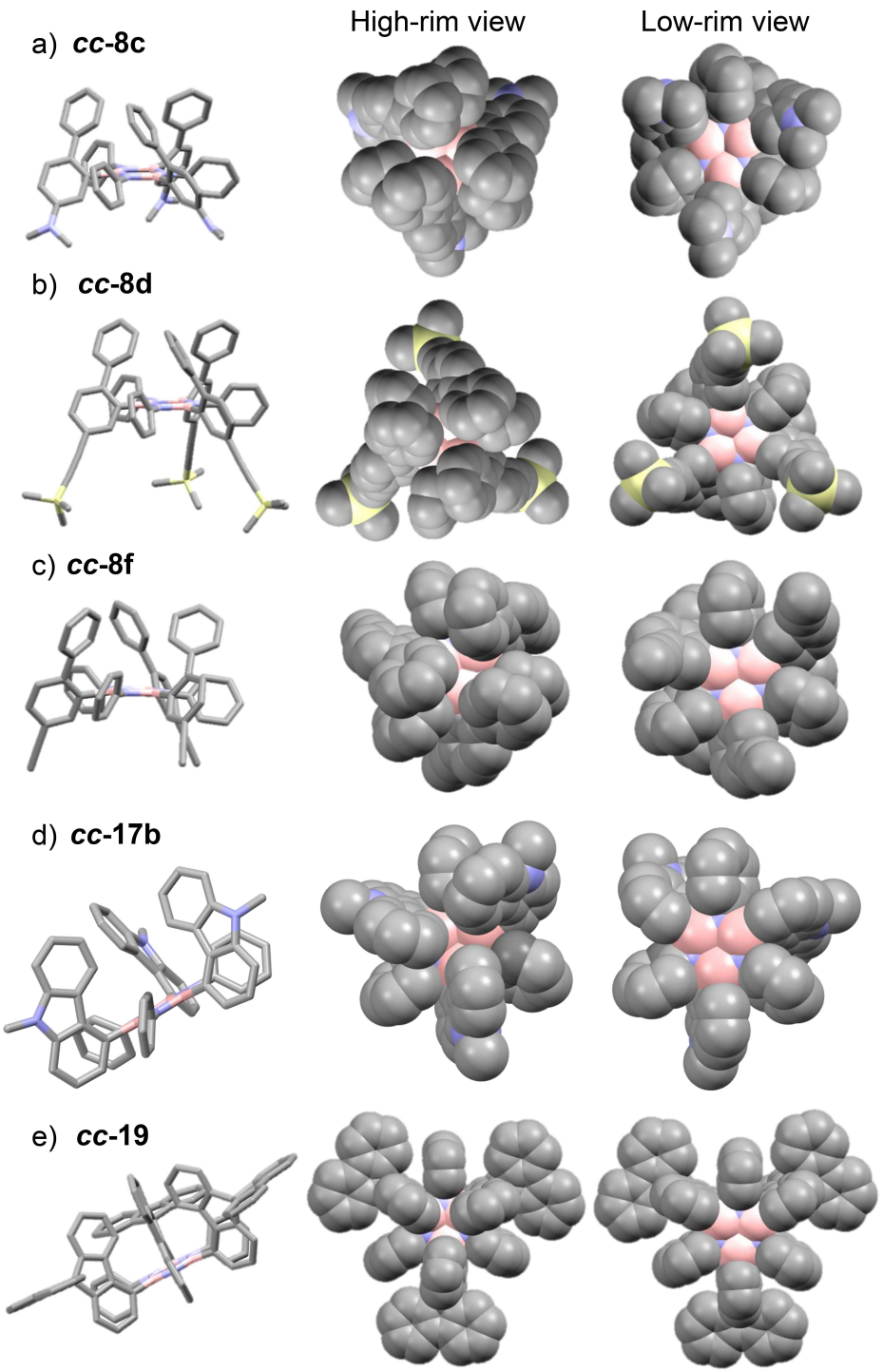

Figure 7. Single-crystal X-ray structure of borazine: a) ***cc*-8c** ($P2_1/c$); b) ***cc*-8d** (*R*-3), c) ***cc*-8f** (*P*-1), d) ***cc*-17b**, ($C2/c$) and e) ***cc*-19** (*Ia*). Crystals were grown by slow diffusion of MeOH in CH_2Cl_2 or slow evaporation from CH_2Cl_2. Grey: C, pink: B, blue: N, and yellow: Si. In *cc*-**17b**, the alkyl chain was excluded for clarity.

multi-redox molecular architecture. With the idea to install electron-active moieties on *cc*-borazines at the late stage in one step with an efficient and atom-economy protocol, we planned to exploit the [2+2] cycloaddition - retro-electrocyclization (CA-RE) reaction between electron acceptor tetracyanoethylene (TCNE) and an alkyne bearing an electron-donating group to prepare a 1,1,4,4-tetracyanobuta-1,3-diene (TCBD) unit as the redox moiety.[25] Capitalizing on the *cis*-directing effect of the phenyl and carbazole moieties, we devised to prepare three-alkynyl derivatives that, upon reaction with TCNE, could give, respectively, a borazine architecture bearing three, spaced far apart, TCBD moieties at the lower rim (***cc*-8g**) and a reference derivative in which three TCBD

© 2024 The Author(s). Angewandte Chemie published by Wiley-VCH GmbH

15213757, 2025, 29, Downloaded from https://onlinelibrary.wiley.com/doi/10.1002/ange.202416700 by Welsh Assembly Government, Wiley Online Library on [21/08/2025]. See the Terms and Conditions (https://onlinelibrary.wiley.com/terms-and-conditions) on Wiley Online Library for rules of use; OA articles are governed by the applicable Creative Commons License

units are sterically congested in the high rim (***cc*-17d**). The structure bearing three TCBD moieties in the high rim is expected to feature a multi-redox behavior, unlike the other architecture where the redox properties will be similar to monomeric TCBD. We commenced the synthesis of ***cc*-8g** preparing borazine ***cc*-8e** (Figure S5.24), using ArLi bearing an *ortho*-phenyl and a *meta*-N,N-dimethylaniline ethynyl moiety (Figure 8a). Because ***cc*-8e** resulted to be unstable under air and on SiO_2, the product was not isolated and the reaction crude subjected to the [2

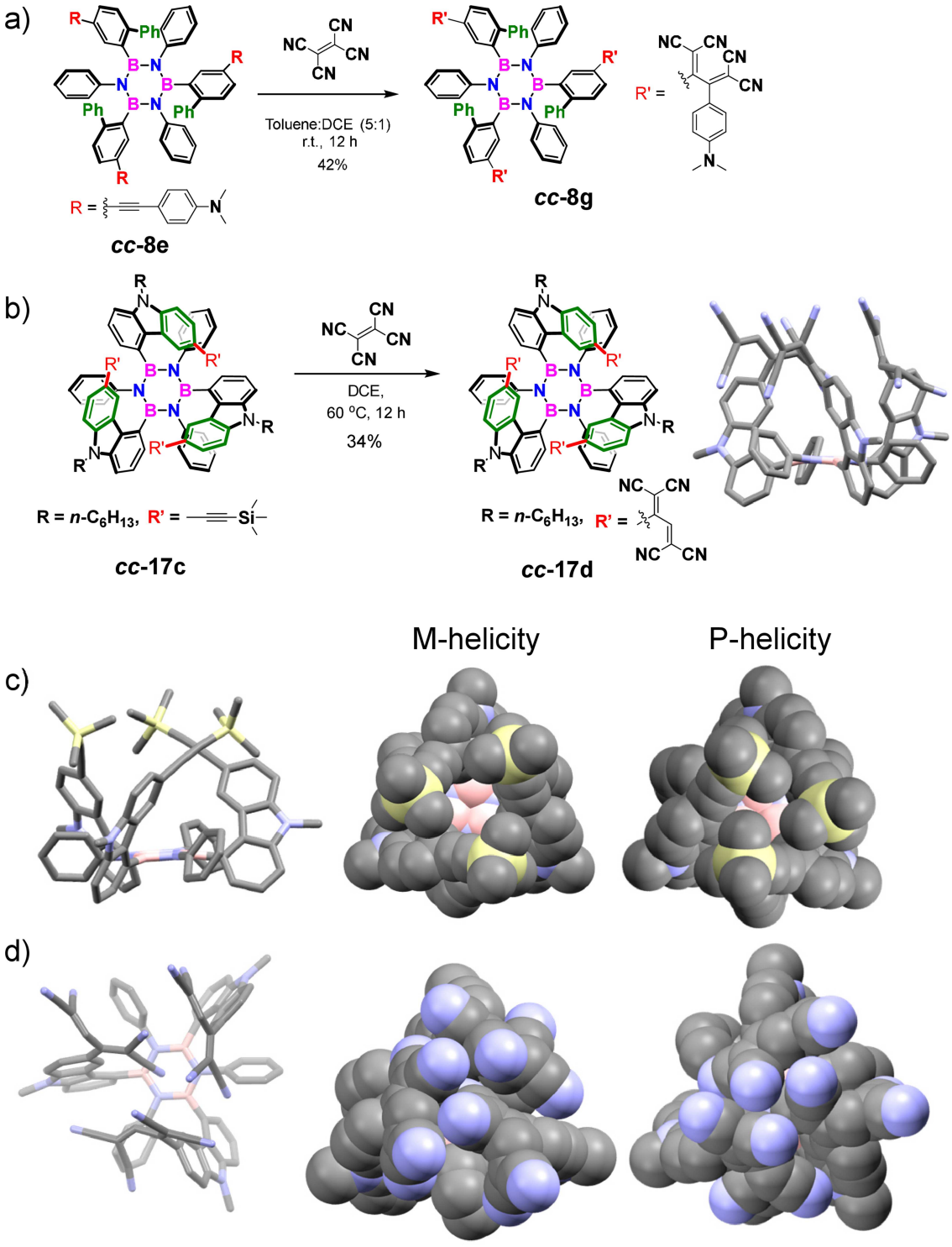

Figure 8. Functionalization of *cc*-substituted borazine derivatives: a) *cc*-**8g** and b) **17d**. Single-crystal X-ray structure of borazines: c) ***cc*-17c** and d) ***cc*-17d**. Crystals were grown by slow evaporation from CH_2Cl_2 or slow diffusion of hexane in CH_2Cl_2 at (−15 °C). Grey: C, pink: B, blue: N, and yellow: Si. The alkyl chain was excluded for clarity.

© 2024 The Author(s). Angewandte Chemie published by Wiley-VCH GmbH

15213757, 2025, 29, Downloaded from https://onlinelibrary.wiley.com/doi/10.1002/ange.202416700 by Welsh Assembly Government, Wiley Online Library on [21/08/2025]. See the Terms and Conditions (https://onlinelibrary.wiley.com/terms-and-conditions) on Wiley Online Library for rules of use; OA articles are governed by the applicable Creative Commons License

+2] cycloaddition reaction with TCNE to give final borazine ***cc*-8g** (Figure 8a). Confirmation of product formation was assessed through mass spectrometry and NMR spectroscopy (Figure S5.25a-d).

Specifically, one proton resonance centered at 3.20 ppm for the -N(Me)$_2$, corresponding to 18 H, suggested the presence of only the *cc*-isomer (Figure S25a). As far as ***cc*-17d** is concerned, tri-ethynyl derivative ***cc*-17c** was first prepared using the carbazole moiety to bias the *cc*-selectivity and place the three trimethylsilyl ethynyl moieties at the higher rim. Single crystal X-ray analysis confirmed the structure of ***cc*-17c**, in which the TMS-ethynyl moieties are arranged in a propeller-like fashion on the high rim.[24] *P* and *M* helicities were observed in the same crystals (Figure S6.8). [2+2] Cycloaddition reaction between ***cc*-17c** and TCNE gave final borazine ***cc*-17d** bearing three TCBD units (Figure 8b), the structure of which was confirmed by mass spectrometry and NMR (Figure S5.35a-d). However, only with single crystal X-ray analysis (Figure 8c) could we unambiguously show the presence of the three sterically congested TCBD groups on the higher rim.[24] As observed for ***cc*-17c**, the ***cc*-17d** also crystallized at the solid state with both *P* and *M* helicities (Figure 8c-d).

Next, we tackled the photophysical and electrochemical characterization of ***cc*-8g** and ***cc*-17d**. Reference TCBD derivatives **15**, **16**, and **20** (Scheme S1) were also prepared for comparison purposes. The steady-state UV/Vis absorption spectrum of ***cc*-8g** featured a CT band at λ_{max} of 397 nm (3.13 eV) with a molar absorptivity (ε) of 69511 M^{-1} cm^{-1} (Figure 9a), that is nearly three times higher than those measured for molecular references **15** and **16** (CT band centered at 379 nm and 468 nm with ε values of 22025 M^{-1} cm^{-1} and 22934 M^{-1} cm^{-1} for derivatives **15** and **16**, respectively, Figures 9b and S7.1-S7.3). When compared to model carbazole-containing TCBD derivative **20**, borazine ***cc*-17d** exhibited a CT band at λ_{max} of 497 nm (2.50 eV) with an ε value of 15885 M^{-1} cm^{-1} (Figures 9c, S7.4 and S7.5). The molecules display a blueshifted CT band with an ε of 5077 M^{-1} cm^{-1} at λ_{max} of 545 nm (2.28 eV). The redox characteristics of substituted borazines and their corresponding model derivatives were investigated through cyclic voltammetry (CV) and differential pulse voltammetry (DPV) in CH_2Cl_2, employing nBu_4NPF_6 (0.1 M) as the supporting electrolyte and the Fc/Fc^+ couple as reference system (Figure 9i). For all reference compounds featuring a single TCBD, two distinct and reversible one-e$^-$ reduction events were

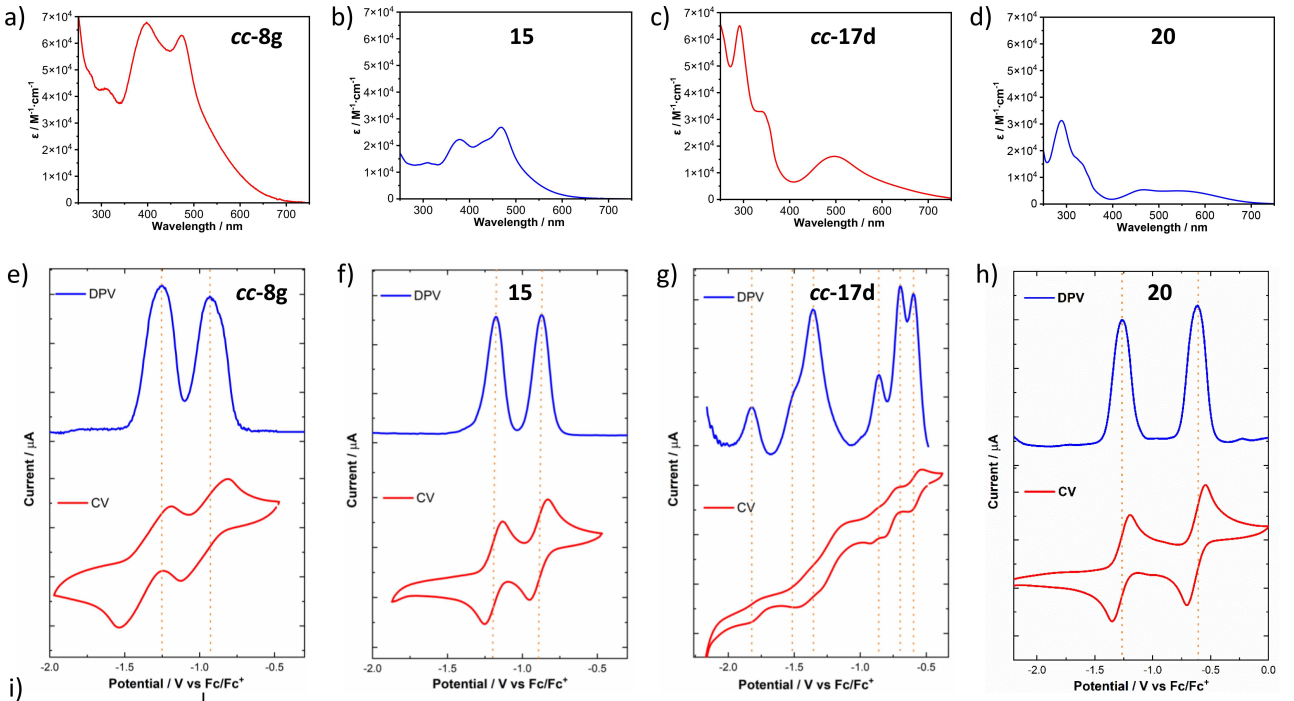

i)

E (V)	E^1_{red}	E^2_{red}	E^3_{red}	E^4_{red}	E^5_{red}	E^6_{red}
***cc*-8g**	-0.958	-1.364	-	-	-	-
15	-0.873	-1.183	-	-	-	-
***cc*-17d**	-0.596	-0.696	-0.857	-1.360	-1.522	-1.819
20	-0.611	-1.271	-	-	-	-

Figure 9. UV-Vis, DPV, and CV measurements of a) ***cc*-8g**, b) **15**, c) ***cc*-17d**, and d) **20** in CH_2Cl_2 (c = 1 mM) with Bu_4NPF_6 (0.1 M) at 100 mV s^{-1} scan rate. e) Electrochemistry data potentials versus the Fc/Fc^+ couple. Working electrode: glassy carbon electrode; counter electrode: Pt; reference electrode: Ag/AgCl.

© 2024 The Author(s). Angewandte Chemie published by Wiley-VCH GmbH

15213757, 2025, 29, Downloaded from https://onlinelibrary.wiley.com/doi/10.1002/ange.202416700 by Welsh Assembly Government, Wiley Online Library on [21/08/2025]. See the Terms and Conditions (https://onlinelibrary.wiley.com/terms-and-conditions) on Wiley Online Library for rules of use; OA articles are governed by the applicable Creative Commons License

observed, centered on the two dicyanovinyl groups (Figure 9f-h, S8.2, S8.3, S8.5). While the electrochemical analysis of borazine ***cc*-8 g** displayed a similar two-reduction profile as that of reference **15** (Figure 9e, S8.1), the electrochemical envelope dramatically changed in the case of borazine ***cc*-17 d** (Figure 9g). As one can discern in the DPV trace of ***cc*-17 d**, six distinctive reductive events appear, of which the first two reduction waves were reversible (Figure S8.4). The study reveals distinct redox behavior influenced by the spatial arrangement of TCBD units in borazines and their model derivatives.

Conclusions

In this paper, we address the synthetic challenges associated with expanding the chemical space of the borazine scaffold by diastereoselectively preparing propeller-shaped hexaphenylborazines that, featuring restricted rotation of the aryl groups, could serve as valuable precursors for constructing complex three-dimensional (3D) C(sp^2)-based architectures. Building on the one-pot, two-step protocol using BCl_3, arylamine, and aryl lithium reagents, we demonstrated that using specific *o*Ss on the organolithium nucleophile one can influence the stereochemistry of the final borazine product. Specifically, it involves using ArLi nucleophiles that, bearing an *o*S, can selectively give access to HABNs featuring all *o*Ss on the same side of the ring (*cc*) or one *o*S exposed opposite (*ct*). Through a detailed systematic study of the stereochemical outcome with different *o*Ss, we recognized that only those *o*Ss featuring a shaft-like (or a stiff-arm-like) structure were capable of fully shielding one side of the borazine ring and giving full *cc*-stereoselectivity in substitution reactions. Notably, this shielding effect transcends classical steric concepts associated with bulkiness, typically correlated with the size of the substituent. The borazine structures were fully characterized through NMR and, whenever possible, with X-ray analyses (fourteen structures were reported). The hypothetical mechanism, stability, and configurational control of these isomers were explored and further confirmed through variable temperature NMR and DFT calculations. Ultimately, the synthesized borazines were leveraged to create multichromophoric molecular architectures, which showed that different optoelectronic properties were obtained depending on the spatial arrangements of the chromophoric units.

The ability to control stereochemistry through judicious choice of *o*Ss opens new avenues for constructing multidimensional architectures. It helps current investigations leave the usual bidimensionality associated with conventional graphenoid systems, design unprecedented three-dimensional sp^2-hybridized structures, and engineer functional materials with tailored properties suitable for catalysis, energy storage, and optoelectronic applications.

Acknowledgements

D.B. gratefully acknowledges the EU through the MSCA-RISE INFUSION (project n° 734834) and IA DecoChrom (project n° 760973) MSCA-ITN-ETN STiBNite (project n° 956923) funding Schemes, Cardiff University and University of Vienna for generous financial supports. Access to the Cardiff University advanced research computing facility (ARCCA) is gratefully acknowledged. MMLG thanks the University of Trieste and Cardiff University for the financial support of her fellowship.

Conflict of Interest

The authors declare no conflict of interest.

Data Availability Statement

The data that support the findings of this study are available from the corresponding author upon reasonable request.

Keywords: borazines · inorganic benzene · boron nitrides · stereoselectivity · optoelectronic properties

[1] M. M. Lorenzo-García, D. Bonifazi, *Chim. Int. J. Chem.* **2017**, *71*, 550–557.
[2] a) D. Bonifazi, F. Fasano, M. M. Lorenzo-Garcia, D. Marinelli, H. Oubaha, J. Tasseroul, *Chem. Commun.* **2015**, *51*, 15222–15236; b) I. Neogi, A. M. Szpilman, *Synthesis* **2022**, *54*, 1877–1907; c) D. Marchionni, S. Basak, A. N. Khodadadi, A. Marrocchi, L. Vaccaro, *Adv. Funct. Mater.* **2023**, *33*, 2303635.
[3] a) M. J. D. Bosdet, W. E. Piers, *Can. J. Chem.* **2009**, *87*, 8–29; b) Z. Liu, T. B. Marder, *Angew. Chem. Int. Ed.* **2008**, *47*, 242–244; c) T. B. Marder, *Chem. Sci.* **2017**, *8*, 846–863; d) M. M. Morgan, W. E. Piers, *Dalton Trans.* **2016**, *45*, 5920–5924; e) H. Helten, *Chem. Eur. J.* **2016**, *22*, 12972–12982; f) X. Y. Wang, J. Y. Wang, J. Pei, *Chem. Eur. J.* **2015**, *21*, 3528–3539; g) M. Stępień, E. Gońka, M. Żyła, N. Sprutta, *Chem. Rev.* **2017**, *117*, 3479–3716; h) A. Narita, X.-Y. Wang, X. Feng, K. Müllen, *Chem. Soc. Rev.* **2015**, *44*, 6616–6643; for some representative examples about doping with B=N: i) S. Nakatsuka, N. Yasuda, T. Hatakeyama, *J. Am. Chem. Soc.* **2018**, *140*, 13562–13565; j) S. Hashimoto, T. Ikuta, K. Shiren, S. Nakatsuka, J. Ni, M. Nakamura, T. Hatakeyama, *Chem. Mater.* **2014**, *26*, 6265–6271; k) M. P. Levinrf, C. Kim, L. Brown, P. Y. Huang, R. W. Havener, D. A. Muller, J. Park, *Nature* **2012**, *488*, 627–632; l) S. R. Wisniewski, C. L. Guenther, O. A. Argintaru, G. A. Molander, *J. Org. Chem.* **2014**, *79*, 365–378; m) M. Krieg, F. Reicherter, P. Haiss, M. Ströbele, K. Eichele, M. J. Treanor, R. Schaub, H. F. Bettinger, *Angew. Chem. Int. Ed.* **2015**, *54*, 8284–8286; n) T. Lorenz, M. Crumbach, T. Eckert, A. Lik, H. Helten, *Angew. Chem. Int. Ed.* **2017**, *56*, 2780–2784; o) O. Ayhan, T. Eckert, F. A. Plamper, H. Helten, *Angew. Chem. Int. Ed.* **2016**, *55*, 13321–13325; p) T. Hatakeyama, K. Shiren, K. Nakajima, S. Nomura, S. Nakatsuka, K. Kinoshita, J. Ni, Y. Ono, T. Ikuta, *Adv. Mater.* **2016**, *28*, 2777–2781; q) A. D. Gorman, J. A. Bailey, N. Fey, T. A. Young, H. A. Sparkes, P. G. Pringle, *Angew. Chem. Int. Ed.* **2018**, *57*, 15802–15806.
[4] A. Stock, E. Pohland, *Berichte Dtsch. Chem. Ges. B Ser.* **1926**, *59*, 2210.

© 2024 The Author(s). Angewandte Chemie published by Wiley-VCH GmbH

15213757, 2025, 29, Downloaded from https://onlinelibrary.wiley.com/doi/10.1002/ange.202416700 by Welsh Assembly Government, Wiley Online Library on [21/08/2025]. See the Terms and Conditions (https://onlinelibrary.wiley.com/terms-and-conditions) on Wiley Online Library for rules of use; OA articles are governed by the applicable Creative Commons License

[5] See some recent advancements in the functionalization of borazines: a) D. Marchionni, A. N. Khodadadi, E. Cela, F. Huang, L. Vaccaro, *Adv. Synth. Catal.* **2023**, *366*, 494–501; b) D. Marchionni, D. Gernini, A. N. Khodadadi, E. Cela, F. Huang, L. Vaccaro, *Green Chem.* **2024**, *26*, 7752–7758; c) A. N. Khodadadi, E. Cela, D. Marchionni, F. Huang, F. Ferlin, L. Vaccaro, *Green Chem.* **2024**, *26*, 7059–7066.

[6] a) H. Noda, M. Furutachi, Y. Asada, M. Shibasaki, N. Kumagai Nature, *Chem.* **2017**, *9*, 571–577; b) J. B. Geri, N. K. Szymczak, *J. Am. Chem. Soc.* **2017**, *139*, 9811–9814; c) J. B. Geri, M. M. Wade Wolfe, N. K. Szymczak, *Angew. Chem. Int. Ed.* **2018**, *57*, 1381–1385.

[7] a) M. Côté, P. D. Haynes, C. Molteni, *Phys. Rev. B* **2001**, *63*, 125207; b) N. A. Riensch, A. Deniz, S. Kühl, L. Müller, A. Adams, A. Pich, H. Helten, *Polym. Chem.* **2017**, *8*, 5264–5268; c) W. M. Wan, A. W. Baggett, F. Cheng, H. Lin, S. Y. Liu, F. Jäkle, *Chem. Commun.* **2016**, *52*, 13616–13619; d) H. Oubaha, N. Demitri, J. Rault-Berthelot, P. Dubois, O. Coulembier, D. Bonifazi, *J. Org. Chem.* **2019**, *84*, 9101–9116; e) J. Dosso, H. Oubaha, F. Fasano, S. Melinte, J. Gohy, C. E. Hughes, K. D. M. Harris, N. Demitri, M. Abrami, M. Grassi, D. Bonifazi, *Chem. Mater.* **2022**, *34*, 10670–10680.

[8] a) K. T. Jackson, M. G. Rabbani, T. E. Reich, H. M. El-Kaderi, *Polym. Chem.* **2011**, *2*, 2775–2577; b) T. E. Reich, S. Behera, K. T. Jackson, P. Jena, H. M. El-Kaderi, *J. Mater. Chem.* **2012**, *22*, 13524–13528; c) T. E. Reich, K. T. Jackson, S. Li, P. Jena, H. M. El-Kaderi, *J. Mater. Chem.* **2011**, *21*, 10629–10632; d) F. Fasano, J. Dosso, C. G. Bezzu, M. Carta, F. Kerff, N. Demitri, B.-L. Su, D. Bonifazi, *Chem. Eur. J.* **2021**, *27*, 4124–4133.

[9] a) C. Huang, C. Chen, M. Zhang, L. Lin, X. Ye, S. Lin, M. Antonietti, X. Wang, *Nat. Commun.* **2015**, *6*, 7698–7704; b) J. Haberecht, A. Krummland, F. Breher, B. Gebhardt, H. Rüegger, R. Nesper, H. Grützmacher, *Dalt. Trans.* **2003**, 2126–2132; c) C. Sánchez-Sánchez, S. Brüller, H. Sachdev, K. Müllen, M. Krieg, H. F. Bettinger, A. Nicolaï, V. Meunier, L. Talirz, R. Fasel, P. Ruffieux, *ACS Nano* **2015**, *9*, 9228–9235.

[10] a) C. Tönshoff, M. Müller, T. Kar, F. Latteyer, T. Chassé, K. Eichele, H. F. Bettinger, *ChemPhysChem* **2012**, *13*, 1173–1181; b) M. Krieg, F. Reicherter, P. Haiss, M. Ströbele, K. Eichele, M. J. Treanor, R. Schaub, H. F. Bettinger, *Angew. Chem. Int. Ed.* **2015**, *54*, 8284–8286; c) J. Dosso, J. Tasseroul, F. Fasano, D. Marinelli, N. Biot, A. Fermi, D. Bonifazi, *Angew. Chem. Int. Ed.* **2017**, *56*, 4483–4487; d) J. Dosso, T. Battisti, B. D. Ward, N. Demitri, C. E. Hughes, P. A. Williams, K. D. M. Harris, D. Bonifazi, *Chem. Eur. J.* **2020**, *26*, 6608–6621; e) E. Fresta, J. Dosso, J. Cabanillas-González, D. Bonifazi, R. D. Costa, *Adv. Funct. Mater.* **2020**, *30*, 1906830; f) M. Fingerle, H. F. Bettinger, *Chem. Commun.* **2020**, *56*, 3847–3850; for an account on the theoretical predictions, see: g) P. Karamanis, N. Otero, C. Pouchan, *J. Am. Chem. Soc.* **2014**, *136*, 7464–7473; h) N. Otero, C. Pouchan, P. Karamanis, *J. Mater. Chem. C* **2017**, *5*, 8273–8287; i) N. Otero, P. Karamanis, K. E. El-Kelany, M. Rérat, L. Maschio, B. Civalleri, B. Kirtman, *J. Phys. Chem.* **2017**, *121*, 709–722; j) L. Caputo, V.-H. Nguyen, J.-C. Charlier *Phys. Rev. Mater.* **2022**, *6*, 114001.

[11] a) A. Narita, X. -Ye Wang, X. Feng, K. Müllen, *Chem. Soc. Rev.* **2015**, *44*, 6616–6643; b) V. Vij, V. Bhalla, M. Kumar, *Chem. Rev.* **2016**, *116*, 9565–9627.

[12] a) Z. Chen, A. Narita, K. Müllen, *Adv. Mater.* **2020**, *32*, 2001893; b) Z. Sun, S. Fang, Y. H. Hu, *Chem. Rev.* **2020**, *120*, 10336–10453.

[13] a) B. Ejlli, P. Nußbaum, F. Rominger, J. Freudenberg, U. H. F. Bunz, K. Müllen, *Angew. Chem. Int. Ed.* **2021**, *60*, 20220–20224; b) D. Ehjeij, F. Rominger, U. H. F. Bunz, J. Freudenberg, K. Müllen, *Angew. Chem. Int. Ed.* **2024**, *63*, e202312040.

[14] a) K. Nagasawa, *Inorg. Chem.* **1966**, *5*, 442–445; b) S. Allaoud, T. Zair, a Karim, B. Frange, *Inorg. Chem.* **1990**, *29*, 1447; c) S. Allaoud, B. Frange, *Inorg. Chem.* **1985**, *24*, 2520–2523.

[15] a) M. Drev, U. Groselj, B. Ledinek, F. Perdih, J. Svete, B. Stefane, F. Pozgan, *Org. Lett.* **2018**, *20*, 5268–5273; b) H. Kwona, E. Lee, *Dalton Trans.* **2018**, *47*, 17206–17210.

[16] a) Y. Yamamoto, K. Miyamoto, J. Umeda, Y. Nakatani, T. Yamamoto, N. Miyaura, *J. Organomet. Chem.* **2006**, *691*, 4909–4917; b) C. A. Jaska, K. Temple, A. J. Lough, I. Manners, *J. Am. Chem. Soc.* **2003**, *125*, 9424–9434; c) W. Luo, P. G. Campbell, L. N. Zakharov, S. Y. Liu, *J. Am. Chem. Soc.* **2011**, *133*, 19326–19329; d) S. Biswas, M. Müller, C. Tönshoff, K. Eichele, C. Maichle-Mössmer, A. Ruff, B. Speiser, H. F. Bettinger, *Eur. J. Org. Chem.* **2012**, 4634–4639.

[17] a) C. A. Brown, A. W. Laubengayer, *J. Am. Chem. Soc.* **1955**, *77*, 3699–3700; b) J. H. Smalley, S. F. Stafiej, *J. Am. Chem. Soc.* **1959**, *81*, 582–586.

[18] a) R. G. Jones, C. R. Kinney, *J. Am. Chem. Soc.* **1939**, *61*, 1378–1381; b) G. E. Ryschkewitsch, J. J. Harris, H. H. Sisler, *J. Am. Chem. Soc.* **1958**, *80*, 4515–4517; c) S. J. Groszos, S. F. Stafiej, *J. Am. Chem. Soc.* **1958**, *80*, 1357–1360; d) A. Wakamiya, T. Ide, S. Yamaguchi, *J. Am. Chem. Soc.* **2005**, *127*, 14859–14866.

[19] a) D. T. Haworth, L. F. Hohnstedt, *J. Am. Chem. Soc.* **1960**, *82*, 3860–3862; b) L. A. Melcher, J. L. Adcock, J. J. Lagowski, *Inorg. Chem.* **1972**, *11*, 1247–1252.

[20] a) S. Kervyn, O. Fenwick, F. Di Stasio, Y. Sig Shin, J. Wouters, G. Accorsi, S. Osella, D. Beljonne, D. Bonifazi, *Chem. Eur. J.* **2013**, *19*, 7771–7779; b) S. Kervyn, N. Kalashnyk, M. Riello, B. Moreton, J. Tasseroul, J. Wouters, T. S. Jones, A. De Vita, G. Costantini, D. Bonifazi, *Angew. Chem. Int. Ed.* **2013**, *52*, 7410–7414; c) N. Kalashnyk, P. Ganeshnagaswaran, S. Kervyn, M. Riello, B. Moreton, T. S. Jones, A. Devita, D. Bonifazi, G. Costantini, *Chem. Eur. J.* **2014**, *20*, 11856–11862; d) D. Marinelli, F. Fasano, B. Najjari, N. Demitri, D. Bonifazi, *J. Am. Chem. Soc.* **2017**, *139*, 5503–5519; e) M. Schwarz, M. Garnica, F. Fasano, N. Demitri, D. Bonifazi, W. Auwärter, *Chem. Eur. J.* **2018**, *24*, 9565–9571; f) J. Dosso, D. Marinelli, N. Demitri, D. Bonifazi, *ACS Omega* **2019**, *4*, 9343–9351.

[21] a) D. Lungerich, D. Reger, H. Hçlzel, R. Riedel, M. M. J. C. Martin, F. Hampel, N. Jux, *Angew. Chem. Int. Ed.* **2016**, *55*, 5602–5605; b) H. Ito, Y. Segawa, K. Murakami, K. Itami, *J. Am. Chem. Soc.* **2019**, *141*, 3–10.

[22] a) G. Domíngueza, J. Pérez-Castells, *Chem. Soc. Rev.* **2011**, *40*, 3430–3444; b) T. D. Leitner, J. S. v Glasenapp, R. Herges, E. Mena-Osteritz, P. Bäuerle, *Adv. Sci.* **2022**, *9*, 2105785; c) T. D. Leitner, Y. Gmeinder, F. Röhricht, R. Herges, E. Mena-Osteritz, P. Bäuerle, *Eur. J. Org. Chem.* **2020**, *2020*, 285–294; d) S. Suzuki, Y. Segawa, K. Itami, J. Yamaguchi, *Nat. Chem.* **2015**, *7*, 227–233; e) S. Batsyts, E. G. Hübner, J. C. Namyslo, M. Gjikaj, A. Schmidt, *Org. Biomol. Chem.* **2019**, *17*, 4102–4114; f) N. M. Alexander, K. Mengele, D. Nauroozi, S. Rau, *Org. Mater.* **2021**, *3*, 295–302.

[23] a) K. S. Choi, M. K. Park, B. H. Han, *Bull. Korean Chem. Soc.* **1999**, *19* 1257–1261; b) L. F. Fieser, *Org. Synth.* **1966**, *46*, 44–45; c) S. Ito, M. Wehmeier, J. D. Brand, C. Kübel, R. Epsch, J. P. Rabe, K. Müllen, *Chem. Eur. J.* **2000**, *6*, 4327–4342.

[24] Deposition Number 1867985 (cc-8a), 1558345 (cc-9), 1558342 (ct-9), 1865297 (cc-10), 1558343 (ct-11), 1865298 (cc-12), 1558344 (cc-13), 2178071 (cc-8c), 2178069 (cc-8d), 2178070 (cc-8f), 2178072 (cc-17b), 2324380 (cc-17c), 2284572 (cc-17d), and 2192822 (cc-19) contains the supplementary crystallographic data for this paper. These data are provided free of charge by the joint Cambridge Crystallographic Data Centre and Fachinformationszentrum Karlsruhe Access Structures service.

[25] a) M. Kivala, F. Diederich, *Acc. Chem. Res.* **2009**, *42*, 235–248; b) T. Michinobu, F. Diederich, *Angew. Chem. Int. Ed.* **2018**, *57*,

© 2024 The Author(s). Angewandte Chemie published by Wiley-VCH GmbH

15213757, 2025, 29, Downloaded from https://onlinelibrary.wiley.com/doi/10.1002/ange.202416700 by Welsh Assembly Government, Wiley Online Library on [21/08/2025]. See the Terms and Conditions (https://onlinelibrary.wiley.com/terms-and-conditions) on Wiley Online Library for rules of use; OA articles are governed by the applicable Creative Commons License

3552–3577; c) T. Michinobu, C. Boudon, J. P. Gisselbrecht, P. Seiler, B. Frank, N. N. P. Moonen, M. Gross, F. Diederich, *Chem. Eur. J.* **2006**, *12*, 1889–1905; d) M. Betou, R. J. Durand, A. Sallustrau, C. Gousset, E. L. Coz, Y. R. Leroux, L. Toupet, E. Trzop, T. Roisnel, Y. Trolez, *Chem. Asian J.* **2017**, *12*, 1338–1346.

Manuscript received: August 30, 2024
Accepted manuscript online: November 12, 2024
Version of record online: June 17, 2025

© 2024 The Author(s). Angewandte Chemie published by Wiley-VCH GmbH

15213757, 2025, 29, Downloaded from https://onlinelibrary.wiley.com/doi/10.1002/ange.202416700 by Welsh Assembly Government, Wiley Online Library on [21/08/2025]. See the Terms and Conditions (https://onlinelibrary.wiley.com/terms-and-conditions) on Wiley Online Library for rules of use; OA articles are governed by the applicable Creative Commons License